ELSEVIER

Catchment soil moisture and rainfall characteristics as determinant factors for discharge/suspended sediment hysteretic loops in a small headwater catchment in the Spanish pyrenees

M. Seeger[a],*, M.-P. Errea[b], S. Beguería[b], J. Arnáez[c],
C. Martí[b], J.M. García-Ruiz[b]

[a]Department of Physical Geography, Faculty of Geography/Geosciences, University of Trier, D-54286 Trier, Germany
[b]Pyrenean Institute of Ecology (CSIC), Campus de Aula Dei, P.O. Box 202, E-50080 Zaragoza, Spain
[c]Department of Physical Geography, University of La Rioja, E-26004 Logroño, Spain

Abstract

The concentration of suspended sediment and discharge generated during flood events are not normally homogenous, and the curve representing sediment concentration vs. discharge through time is often a hysteretic loop. Three types of hysteretic loops were found at Arnás, a Mediterranean headwater catchment in the Central Spanish Pyrenees: clockwise (the most frequent), counter-clockwise and eight-shaped. They are associated with different levels of humidity and rainfall and therefore indicators of different processes of runoff and sediment transport. Clockwise loops are generated under 'normal' stormflow conditions, when the catchment is very moist and runoff generation and sediment supply is limited to areas next to the channel (i.e. sediments are removed, transported and depleted rapidly). Counter-clockwise curves occur under very high moisture and high antecedent rainfall conditions. In this case, flood propagation occurs as a kinematic wave. Sediment sources are incorporated all over the catchment. In both cases, saturation excess overland flow generates the superficial runoff. The eight-shaped loop (partial clockwise followed by counter-clockwise) occurs with low water content. Here, the runoff generation process is supposed to be infiltration excess overland flow, which causes a rapid extension of the contributing areas both near the channel and over the whole catchment.
© 2003 Elsevier B.V. All rights reserved.

1. Introduction

In naturally vegetated headwater catchments, suspended sediment is normally transported during flood events. However, the relation between suspended sediment concentration (SSC) and discharge (Q) is not normally homogenous during the event,

* Corresponding author.
E-mail addresses: seeger@uni-trier.de (M. Seeger), paz@ipe.csic.es (M.-P. Errea), sbegueria@ipe.csic.es (S. Beguería), jose.arnaez@dchs.unirioja.es (J. Arnáez), cmarti@ipe.csic.es (C. Martí), humberto@ipe.csic.es (J.M. García-Ruiz).

often producing hysteretic loops. Systematic exploration of possible Q-SSC relationships concluded that there are five common classes of hysteretic loops (Williams, 1989): single valued, clockwise, counter-clockwise, single valued plus a loop and eight-shaped. Even though this classification includes data and causal explanations, hysteresis is still regarded as a problem. For example, it generates a large scatter of runoff-sediment discharge data for complete flood events (Hodkins, 1999; Batalla and Sala, 1994) or only a partially significant correlation between SSC and Q (Chikita et al., 2002). Recent publications have identified sediment sources by systematically analysing single event hysteretic loops of sediment transport (diCenzo and Luk, 1997; Lenzi and Marchi, 2000; Jansson, 2002) or identifying different runoff processes by describing hysteresis in temperature and specific conductance (Kobayashi et al., 1999). Hysteresis is also controlled by catchment size, rainfall amount and soil moisture (Klein, 1984; DeBoer and Campbell, 1989).

Soil water content is one of the most important factors for the generation of runoff. It affects infiltration capacity and the capability of soils to store new rainfall water, as reflected in many physically based hydrological models (Bronstert, 1994; Bronstert et al., 1998). For this reason, the different runoff generating processes (saturation excess overland flow, infiltration excess overland flow and even return flow) are highly regulated by soil characteristics and especially by soil moisture, and not by precipitation characteristics. The response of a small catchment to precipitation will greatly depend on moisture conditions within the catchment.

In catchments in Mediterranean mountain areas many hydrological and geomorphic processes occur with changing temporal dominance due to the high temporal and spatial variability of rainfall and evapotranspiration and the spatial variability of mainly degraded soils. As a result, it is difficult to find general rules that explain or predict runoff generation and suspended sediment transfer (Lorente et al., 2000; García-Ruiz et al., 2000; Gallart et al., 1998). For this reason, the study of hysteretic loops in Mediterranean headwater catchments has progressed from the description of a singular event (Llorens et al., 1997) to the separation of rainfall-runoff events by

investigating hysteretic loop types (Regüés et al., 2000) and the consequent characterisation of the processes. In Eastern Pyrenean catchments with abandoned agricultural activity, Regüés et al. (2000) identified (1) clockwise hysteretic loops with low sediment concentrations, mainly at the end of the dry period and (2) counter-clockwise loops with high sediment concentrations at the end of the moist period. They explained the occurrence of both according to different sediment sources and runoff generating areas.

In this study we identify and classify the different hysteresis types of the Q-SSC relationships of single flood events and the relationships between the hysteresis types and the conditions for runoff generation. The central aim was to understand the factors leading to the discharge-sediment transport patterns. The identification of different types of hysteretic loops and their generation conditions may indicate the dominance of different runoff generating processes.

2. The study area

The Arnás catchment is located in the Upper Aragón River Basin, a northern tributary of the Ebro River (Fig. 1). The bedrock is Eocene Flysch with alternating sandstones and marl layers sloping northward, which is characteristic of a wide sector of the Central Spanish Pyrenees.

The climate is mountainous Mediterranean with a strong oceanic influence, especially in winter. The average annual precipitation is about 1100 mm, mostly concentrated from October to May but divided by a secondary minimum in March. The average annual temperature is 10 °C.

The Arnás ravine drains a 284 ha headwater catchment into the Lubierre River, a small tributary of the Aragón River. The highest peak is at 1330 m a.s.l. with the outflow at about 900 m a.s.l. The ravine runs from west to east, building up a valley with a strong contrast between the steep south facing slope and the gentle north facing slope.

The morphology of the slopes is characterised by big rotational landslides and earthflows. On the south facing slope there are some old and active debris-flows. Some poorly drained areas can be found related
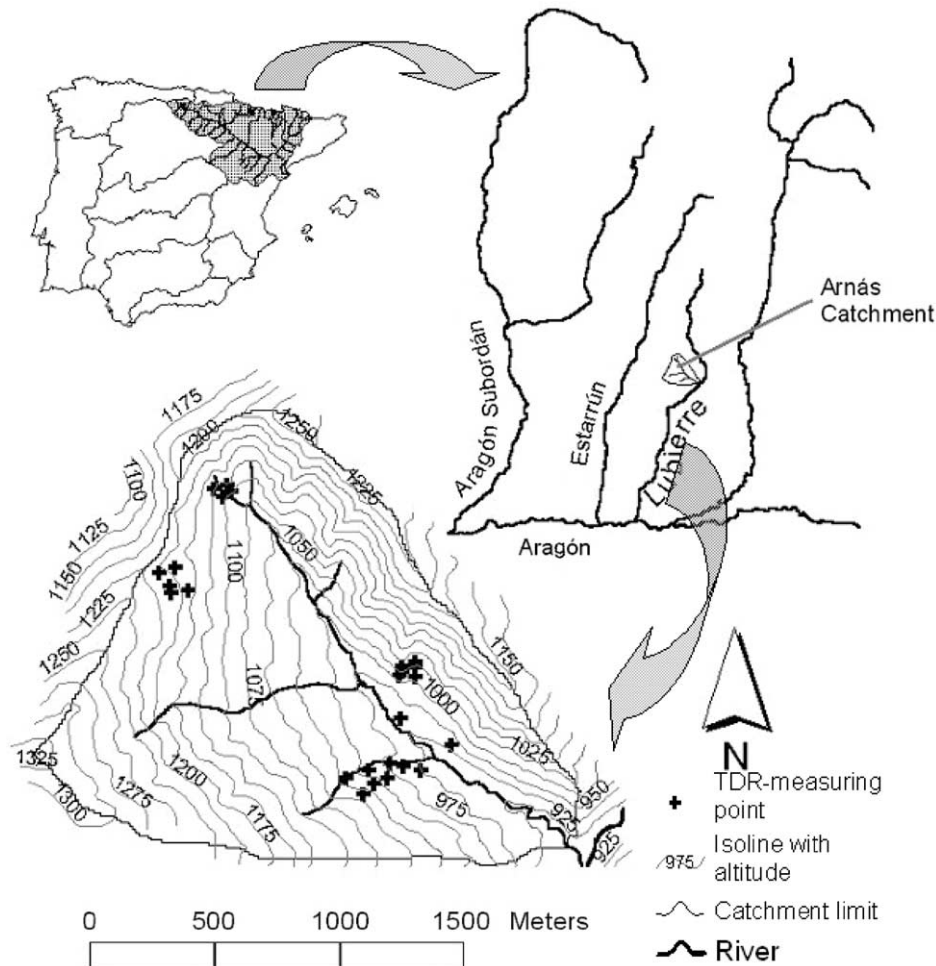
Fig. 1. Location of the Arnás catchment.

to the rotational landslides, especially in the shady aspect. They are mostly disconnected from the drainage network.

Due to former land-use (mainly cereal crops, even on the steep and convex slopes, which were completely abandoned in the middle of the 20th century), the soils on the south-facing slope are mostly poorly developed, shallow carbonate-rich Regosols (FAO, 1998). Deeper and more differentiated soils such as Cambisols and Calcisols can only be found on the terraced concave slopes. At the valley bottom stagnic conditions are predominant even on shallow stony soils due to the poor drainage capacity of the clayey fine material. The soils in these areas are Stagnic or Vertic Cambisols and Calcisols.

The soils on the north-facing slope are more developed because they are less steep, have a more dense vegetation cover, and accumulate more organic material. The predominant soil types are Kastanozems which may also be strongly influenced by stagnant water and accumulation and erosion processes on the terraces. All soils have a low infiltration capacity, decreasing below 5 mm h^{-1} when moist, as a result of the high clay content. Saturated hydraulic conductivity tends to decrease with soil depth (Seeger, 2001).

The soil matrix is highly erodible, but often protected by a stone layer. However, there is a permanent transport of material to the surface due to the high activity of soil invertebrates which provide new erodible material to the whole catchment.

Most of the catchment is covered by shrubs, *Genista scorpius*, *Buxus sempervirens* and *Rosa canina*. The highest areas have been colonised by *Pinus silvestris* and *Quercus faginea*. Due to sheep grazing, the vegetation succession is strongly retarded and absent on many trails (Ries et al., 2000).

Runoff reaches the flume rapidly after precipitation, and the shape of the hydrograph reflects the precipitation structure. However, only the maximum rainfall intensity of the storm is significantly correlated with the amount of stormflow discharge or the total discharge (Arnáez et al., 1999). The discharge is normally free of suspended sediment and has a low conductivity (around 340 μS cm^{-1} at 25 °C), which is considerably lower during flood events. The major dissolved components are Calcium cations and carbonates.

3. Equipment and methods

The catchment is equipped with a rectangular flume with a maximum capacity of 3 m^3 s^{-1}:

- Water height is measured by an ultra-sound sensor (Lundhal DCU-7110).
- Suspended sediment load is measured by turbidity meter (LYX 8000 PT1).
- Conductivity is measured with a Dr Lange conductivity meter without temperature correction (which is performed afterwards).

The first two parameters are collected every 5 min, the last one every 15 min. In addition, an automatic sampler was installed to start sampling the water in the flume at a height of 30 cm (660 l s^{-1}), at the same place where turbidity is measured. The samples are analysed in laboratory and the concentration of suspended sediment has been used to calibrate the turbidity sensor.

Meteorological data (radiation, air temperature and wind-speed) are stored every 15 min, except rainfall that is registered every 5 min. A second rainfall gauge has been installed on the upper part of the Arnás catchment. The data recorded at both gauges are practically identical, demonstrating that rainfall events are very homogenous in the catchment.

Soil moisture has been measured with a Tektronix cable tester with 20 cm probes at 25 sites in the catchment that have been selected according to topographical features (south and north facing slopes, concave and convex slopes, etc.). Measurements were taken once a week except in winter.

Potential evapotranspiration (ETP) was calculated after Hargreaves and Samani (1985) using the temperature data of the meteorological station at the catchment. We calculated the average of the soil moisture measurements for characterising the catchment moisture status, excluding anomalous values from one site. All other measuring points are highly correlated ($r^2 > 0.8$). Normally, no measurements have been taken during flood events. For this reason soil moisture was interpolated following Sauer and Ries (2002), based on the measured precipitation and the calculated ETP. Soil water balance was calculated based on Thornthwaite and Mather (1957), Pfau (1966), Lanfer (1995), Havans (1956) and Hargreaves and Samani (1985), assuming no direct superficial runoff and applying an empirical formula for the real evaporation from soils depending on the soil moisture. Percolation of exceeding water into deeper zones was also included. Afterwards, the interpolation has been calibrated with the measured data.

The rainfall-runoff events are characterised by three groups of variables:

1. The rainfall causing every event is characterised by its total amount (P, mm), average intensity (IP, mm h^{-1}) and maximum rainfall in 5 min ($IP5$, mm) and 30 min ($IP30$, mm).
2. The conditions prior to the flood are described by the rainfall 6 h ($AP6$), 24 h ($AP1d$) and 3, 7, 15 and 21 days before ($AP3d$, $AP7d$, $AP15d$, $AP21d$ respectively). In addition, the average discharge 24 hours before the beginning of the flood ($AQ24h$) is calculated for every rainfall-runoff event. In this group of variables, the interpolated soil moisture value is included.
3. The runoff peak is characterised by the average discharge of the flood (Q, l s^{-1}) and the maximum discharge in 5 and 30 min (Q_5 and Q_{30}, l s^{-1}). The contribution of baseflow to the total peak has been determined by a linear baseflow separation (Hewlett and Hibbert, 1967). The characteristics of sediment transport are

described in a similar way, using the average concentration (*SSC*, mg l^{-1}) and the maximum concentration in 5 and 30 min (*SSC5* and *SSC30*, mg l^{-1}).

To classify the floods in relation to their hysteretic loop, *Q-SSC* graphs were drawn with linear axes for both variables. The classification was made graphically according to some of the classes established by Williams (1989): clockwise, counter-clockwise and eight-shaped hysteretic loops.

After evaluating the descriptive statistics, canonical discriminant analysis (CDA) was performed with the SPSS program package using the variables of the first two groups mentioned above (i.e. the variables considered to cause of the flood). The variables of the long term antecedent rainfall (*AP15d*, *AP21d*) were not included to avoid loosing a large part of the sample due to missing values. Group separation was performed using the Mahalanobis distance from centroid as a criterium. The test for consistency of the classification was carried out by cross validation.

After the CDA, an ANOVA with a Dunnet-T3 post-hoc test was performed with the variables selected for the discriminant functions, to test the differences between the groups for the single variables.

4. Results

During the soil moisture monitoring in 1997, 19 flood events were recorded (Fig. 2). Twelve of them were classified as clockwise (c) (Fig. 3), three as counter-clockwise (a) (Fig. 4) and the remaining four as eight shaped (e) (Fig. 5) where a clockwise loop at low discharges changes into a counter-clockwise loop at high discharges. This last group occurred only during July and August, when soil moisture was predominantly very low. Clockwise and counter-clockwise events were registered throughout the year, the latter always following one or more of the first ones. A summary of the data from the events is presented in Table 1.

The precipitation (*P*) that caused the floods oscillated between 3.4 and 47.8 mm. The intensity of the rainfalls ranged from 0.4 to 11.6 mm in 5 min (*IP5*), whereas the average rainfall intensity (*IP*) was between 1.2 and 20.8 mm h^{-1}. The antecedent rainfall ranged from no rain to 109 mm during the 7 days prior to the stormflow (*AP7d*). The highest precipitation 6 h (*AP6h*), 1 day (*AP1d*) and 3 days before the event (*AP3d*) were 18.4, 71.2 and 86.8 mm respectively.

The floods analysed included a wide range of discharge characteristics. The average discharge (*Q*)
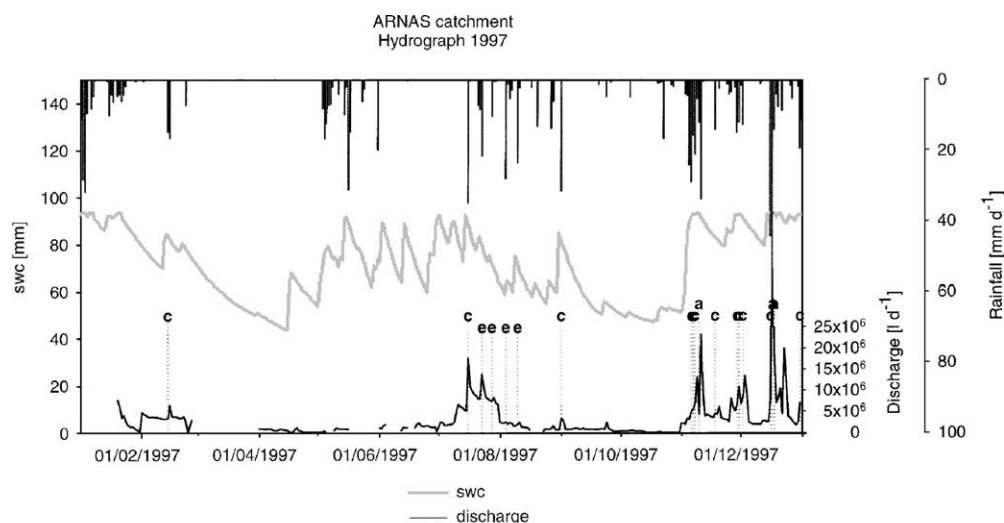

Fig. 2. Hydrograph of 1997, including modelled soil water content (SWC) and daily rainfall. Stormflow events are marked with hysteretic classification (c-clockwise, a-counter-clockwise, e-eight shaped).
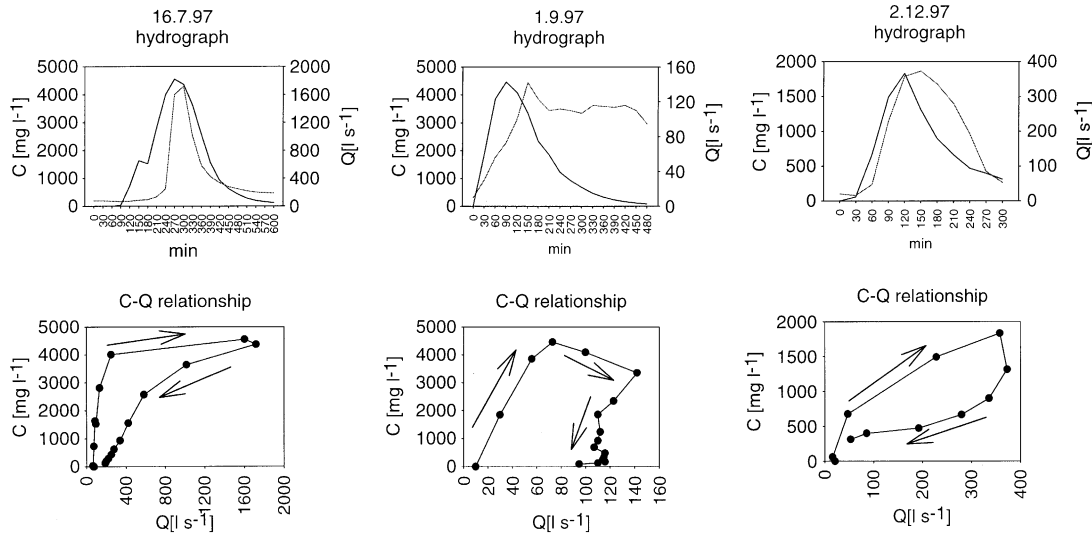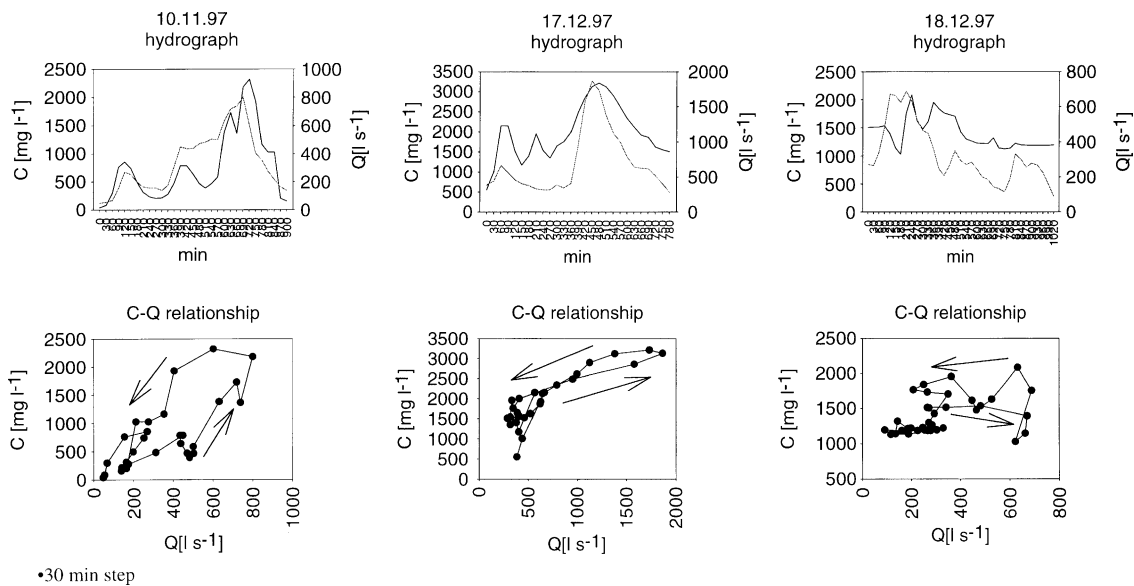
Fig. 3. Examples of clockwise hysteretic loops, corresponding to the events of 16/7, 1/9 and 2/12/1997. Upper figure is hydrograph and sedigraph, lower figure the Q-SSC relationship during the flood event.

ranged from 47.6 to 701.7 $l\,s^{-1}$, corresponding to peak discharges ($Q5$) between 86.9 and 2347 $l\,s^{-1}$. The runoff coefficient (RC) was 0.17 for all floods, but varied between 0.01 and 0.70, with an average contribution of baseflow ($BF\%$) to the stormflow of 34.3% (range = 8.9–74.7%). The characteristics of sediment transport were also scattered. The average

suspended sediment concentration (SSC) reached from 34.9 to 2288.6 mg l^{-1} with peak values ($SSC5$) between 86 and 4780.7 mg l^{-1}. The floods were generated at water contents of the upper 20 cm of the soil (SWC) between 58.4 and 93.4 mm, with an average of 86.4 mm, which is higher than field capacity.

•30 min step

Fig. 4. Examples of counter-clockwise hysteretic loops, corresponding to the events of 10/11, 17/12 and 18/12/1997. Upper figure is hydrograph and sedigraph, lower figure the Q-SSC relationship during the flood event.
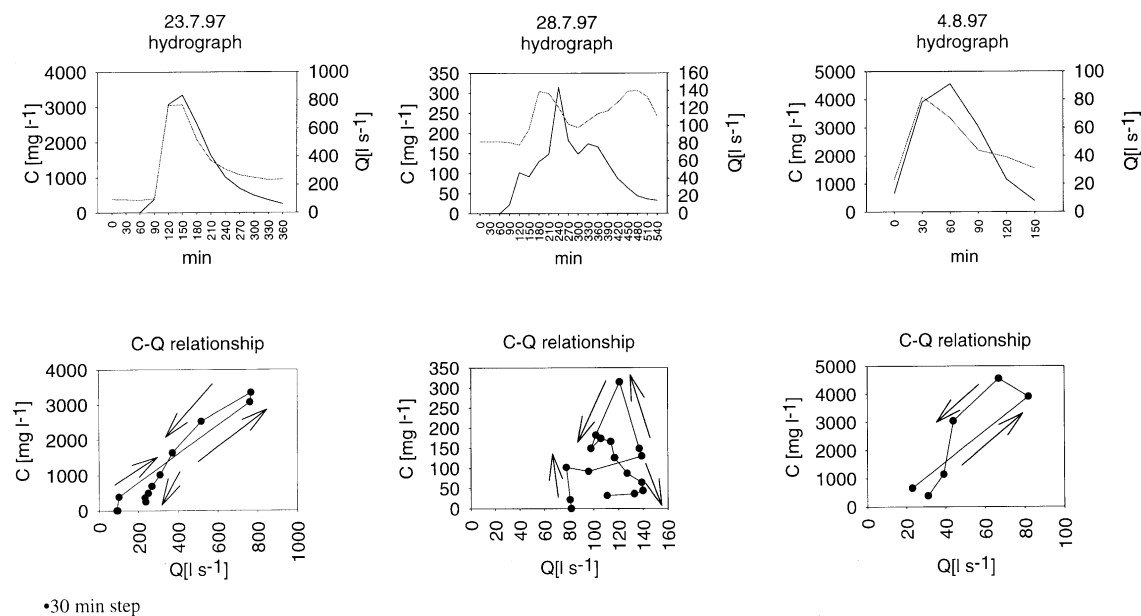
Fig. 5. Examples of eight-shaped hysteretic loops, corresponding to the events of 23/7, 28/7 and 4/8/1997. Upper figure is hydrograph and sedigraph, lower figure the Q-SSC relationship during the flood event.

The main differences of the three flood types in the rainfall, discharge and sediment transport characteristics are documented in Table 1.

All the hydrographs reflect the characteristic fast response of the catchment to precipitation (Figs. 3–5), but: (i) counter-clockwise shaped stormflow events were characterised by long duration, especially of the sediment transport, and an irregular evolution of the hydrographs and the hysteresis loops; and (ii) eight-shaped events are commonly short stormflows with a heterogeneous evolution of the sediment discharge. Despite the wide range of discharge and sediment transport parameters, the clockwise shaped events had a clear recognisable hysteretical behaviour, and hydrographs and sedigraphs can be described as typical (see Arnáez et al., 1999; García-Ruiz et al., 2000).

The discriminant analysis created two canonical discriminant functions including three of the input variables to separate the groups (Table 2, Fig. 6): total rainfall (P), antecedent rainfall 3 days before the event ($AP3d$), and soil moisture on the day of the event (SWC). The first canonical discriminant function (f1) explained nearly 80% of the variance (Table 2) and was highly positively correlated with SWC (0.957) and only slightly correlated with the other variables. For this reason, f1 expresses increasing soil water content in the catchment at the time of the floods with higher function values. The second discriminant function (f2) correlated with the resting parameters but very much lower (0.542 for $AP3d$ and 0.443 for P), as expected by the lower proportion of variance explained. Its standardised coefficients (Table 2) represent the precipitation height and especially the antecedent rainfall three days before the event, where the function value is higher with increasing parameter values. Also, f2 increases with decreasing SWC, but with very low intensity.

Table 2 also contains the discriminant function values at the centroids of the three flood types. The distribution of the flood events in the two dimensions created by the functions is shown in Fig. 7 (discriminant function coefficients are shown in Table 2). The centroid of the clockwise flood group was close to 0 in both functions (f1 = 0.654; f2 = -0.652). The other groups represent opposite extremes during the flood generation rainstorms. The counter-clockwise centroid had

Table 1
Characteristics of the analysed rainfall-runoff events. Not all listed variables have been used for the analysis

	All floods					Clockwise (c)					Counter-clockwise (a)					Eight-shaped (e)				
	N	Min	Max	Avg	SD	N	Min	Max	Avg	SD	N	Min	Max	Avg	SD	N	Min	Max	Avg	SD
P	19	3.4	47.8	21.3	12.3	12	3.4	47.8	19.1	13.3	3	28.9	37	34.1	4.5	4	11.0	27.6	18.5	7.3
IP30 (mm)	19	1.6	20.6	6.2	5.8	12	1.6	15.6	4.3	4.1	3	2.6	8.6	4.7	3.4	4	3.6	20.6	12.7	7.9
IP5 (mm)	19	0.4	11.6	2.3	3.0	12	0.4	5.6	1.5	1.6	3	0.6	0.8	0.7	0.1	4	0.8	11.6	5.7	5.0
IP	19	1.2	20.8	4.6	5.0	12	1.2	12.7	3.4	3.3	3	2.5	2.9	2.7	0.2	4	2.9	20.8	9.8	8.2
AP6h	19	0	18.4	4.0	5.0	12	0	8.6	2.9	3.1	3	2.4	18.4	10.7	8.0	4	0	9.4	2.4	4.7
AP1d	19	0	71.2	14.3	20.2	12	0	39.4	9.5	11.4	3	9	71.2	46.1	32.8	4	0	12.4	5.0	6.1
AP3d	18	0	86.8	25.9	26.8	11	0	62.2	23.2	23.7	3	38.2	86.8	61.0	24.4	4	0	16.6	7.3	8.5
AP7d	18	0	109.6	39.3	32.2	11	0	82.2	31.1	27.9	3	60.2	109.6	86.1	24.8	4	11.8	47	26.8	15.5
AQ24h	19	3.1	576.2	128.5	149.0	12	3.1	359.1	91.8	98.5	3	202.8	576.2	372.1	189.1	4	14.4	93.7	55.8	41.2
Q	19	47.6	701.7	199.1	167.0	12	61.1	376.5	157.6	107.4	3	328.6	701.7	455.9	212.9	4	47.6	314.4	131.1	125.5
Q30	19	81.5	1865.0	475.7	533.3	12	82.6	1716.2	383.9	470.5	3	688.5	1865.0	1117.9	649.4	4	81.5	767.2	269.5	332.8
Q5	19	86.9	2347.1	545.4	652.5	12	86.9	2347.1	445.6	639.9	3	716.4	1947.3	1161.4	682.6	4	90.4	1185.1	382.4	535.9
BF%	19	8.9	74.7	34.3	20.6	12	11.0	69.4	34.1	20.7	3	8.9	26.3	17.6	8.7	4	29.3	74.7	47.3	20.4
RC	19	0.01	0.70	0.17	0.16	12	0.04	0.70	0.18	0.18	3	0.18	0.42	0.27	0.13	4	0.01	0.12	0.07	0.06
SSC	19	34.9	2288.6	730.9	698.5	12	34.9	1533.4	488.3	525.9	3	759.2	1980.6	1381.3	611.0	4	98.4	2288.6	970.9	963.8
SSC30	19	86.0	4558.1	1823.7	1537.5	12	86.0	4549.3	1465.7	1547.8	3	2085.4	3212.6	2539.3	594.7	4	315.2	4558.1	2361.0	1937.3
SSC5	19	86.0	4780.7	1926.4	1549.2	12	86.0	4583.4	1570.3	1554.2	3	2193.0	3212.6	2575.2	555.6	4	335.4	4780.7	2508.1	1989.6
SWC	19	58.4	93.4	86.4	9.7	12	82.0	93.4	89.8	4.2	3	93.4	93.4	93.4	0.0	4	58.4	80.5	70.8	9.1

Table 2
Data of the canonical discriminant functions (cdf)

	Function	1	2
Canonical function coefficients	P	0.316	0.779
	AP3d	0.141	1.008
	SWC	0.946	− 0.478
Eigenvalues of cdf	Eigenvalue	3.714	1.023
	Variance (%)	78.4	21.6
	Accumulated variance (%)	78.4	100.0
	Canonical correlation	0.888	0.711
Structure matrix of cdf	**SWC**	**0.957**	− 0.229
	IP	**0.330**	*0.160*
	AP3d	0.339	**0.542**
	AQ24h	*0.408*	**0.487**
	P	0.148	**0.443**
	IP30	*0.091*	**0.385**
	AP1d	*0.186*	**0.340**
	AP7d	*0.287*	**0.292**
	AP15d	− *0.144*	− **0.285**
	AP21d	− *0.132*	− **0.246**
	AP6h	*0.110*	**0.240**
	IP5	*0.149*	**0.209**
cdf coeficients	P	0.028	0.068
	AP3d	0.006	0.046
	SWC	0.189	*0.096*
	(const.)	− 17.151	5.612
Group centroids	c	0.654	*0.652*
	a	1.856	1.820
	e	− 3.189	0.427

The table shows standardised canonical function coefficients of the variables included in the analysis, eigenvalues of the canonical discriminant functions and the structure matrix of the canonical discriminant functions. Here the highest correlations of the variables with the functions are signed bold, all variables excluded in the analysis are signed italic. The fourth part of the table contains the canonical discriminant function coefficients, the last part of he table includes the group centroids.

relatively high values for both functions (f1 = 1.856; f2 = 1.820). These floods were generated under very high moisture conditions and with high rainfall and antecedent rainfall. The distribution of the single flood events (Fig. 5) suggests that they depended on the antecedent and actual rainfall, whilst soil moisture was invariant; during the counter-clockwise shaped events soil water content was the same at saturation level (see Table 1). The eight-shaped events had an extremely low f1
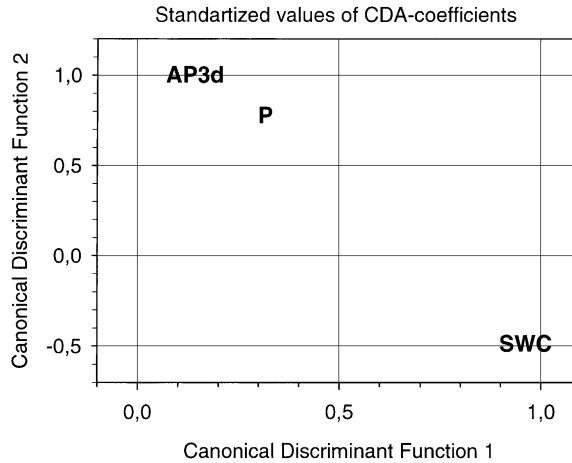

Fig. 6. Standardised discriminant function coefficients of the variables included into de discriminant functions. Values correspond to Table 2.

(− 3.189) and were close to zero for f2 (0.427). That is, the eight shaped flood events were generated especially under dry conditions, but with no special rainfall characteristics. According to the distribution of the events along the f1-axis, the soil moisture determined this type of stormflows.

Examining the measured values of the discriminant factors in detail (Table 1), we can observe that the total precipitation that caused counter-clockwise hysteretic loops is, with an average of 34.1 mm, considerably higher than the ones that caused the other
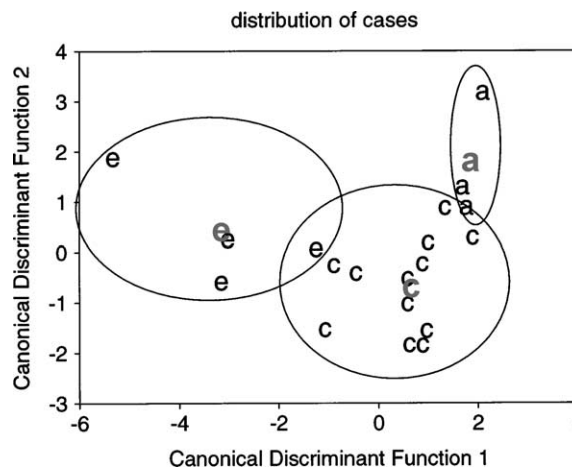

Fig. 7. Distribution of cases with discriminant functions.

Table 3
Post-Hoc test Dunnet-T3 to the ANOVA of the factors included in the discriminant functions. Significant variables are marked bold

Group	Group	Factor	Avg. diff.	Avg. error	Sig.
c	a	P	**− 16.1**	4.3	0.01
		AP3d	− 39.5	15.6	0.19
		SWC	**− 3.2**	1.1	0.03
	e	P	− 0.4	5.0	1.00
		AP3d	14.3	8.0	0.25
		SWC	**19.3**	4.7	0.05
a	c	**P**	**16.1**	4.3	0.01
		AP3d	39.5	15.6	0.19
		SWC	**3.2**	1.1	0.03
	e	**C**	**15.7**	4.5	0.05
		AP3d	53.8	14.7	0.11
		SWC	**22.5**	4.6	0.04
e	c	P	0.4	5.0	1.00
		AP3d	− 14.3	8.0	0.25
		SWC	**− 19.3**	4.7	0.05
	a	P	− 15.7	4.5	0.05
		AP3d	− 53.8	14.7	0.11
		SWC	**− 22.5**	4.6	0.04

flood events. The values for clockwise and eight-shaped events are very similar, around 19 mm. In contrast, the antecedent rainfall (*AP3d*) is lowest for the eight shaped events (7.3 mm) and highest for the counter-clockwise shaped events (61.0 mm). But again, eight-shaped and clockwise shaped flood events are similar in their wide range of precipitation prior to the floods: in both cases there were observed events without antecedent precipitation.

The soil water content (*SWC*) shows a different situation. Here, clockwise and counter-clockwise shaped floods occurred with the soils at a high moisture content (89.8 and 93.4 mm, respectively), whilst eight shaped floods show low soil humidity conditions (70.8 mm). It is remarkable that all eight shaped events were generated with dryer soil conditions than all the other events, and counter-clockwise shaped events have no variability of soil moisture.

The Dunnet-T3 test (Table 3) shows how each of the extracted factors is able to differentiate the three types of sediment transport. The differences of the antecedent rainfall are not significant for separating the three groups. The total rainfall amount is only significant as a differentiating factor for the counter-clockwise shaped hysteretic loops from the other two types. Only the soil water content is able to state the differences between all groups. The *p*-value for the differentiation of the clockwise loop from the eight-shaped loop is only slightly higher than 0.05, for this it is considered in this case as significant.

In the discriminant functions (Table 4), only one of the eight-shaped floods was wrongly classified as a clockwise shaped flood. The cross-validation results were also very good. One counter-clockwise and one eight-shaped group were classified as clockwise and two clockwise were placed in the counter clockwise group.

5. Discussion and conclusions

We identified three types of flood events according to the *Q-SSC* hysteretic loops, with substantial differences in discharge, sediment transport and rainfall conditions.

Table 4
Classification statistics and cross validation for canonical discriminant functions. Absolute values and percentage (in brackets)

	Hysteresis	Prognostized group			Total	Correct classified
		r	*l*	*e*		
Original	c	12 (100%)	0 (0%)	0 (0%)	12 (100%)	95.00%
	a	0 (0%)	3 (100%)	0 (0%)	3 (100%)	
	e	1 (25%)	0 (0%)	3 (75%)	4 (100%)	
Cross-validation	c	10 (83%)	2 (17%)	0 (0%)	12 (100%)	79.00%
	a	1 (33%)	2 (66%)	0 (0%)	3 (100%)	
	e	1 (25%)	0 (0%)	3 (75%)	4 (100%)	

Clockwise hysteresis is the most common, with low suspended sediment concentration and high superficial runoff coefficients. As indicated by Williams (1989) and confirmed by Regüés et al. (2000) for a Mediterranean mountain catchment, the rapid increase in *SSC* at the beginning of the flood event is explained by a rapid displacement of the sediment from sources near the channel— the 'bulldozer' effect (Regüés et al., 2000). The decrease of *SSC* before the decrease of *Q* indicates that the sediment sources are limited and rapidly depleted. Therefore, the runoff generation (and sediment mobilisation) is limited to areas near the channel. In counter-clockwise hysteretic loops, the *SSC* peak reaches the flume after the peakflow. This may be due to the travel distance from the runoff and sediment generating areas since discharge peaks can travel with wave velocity to the gauging station, whereas the suspended sediment travels with flow velocity (Williams, 1989) and sediments are transported from areas that are far away from the channel. Another reason is the retarded incorporation of sediment sources to the stormflow event, as described by Threlfall (1986) for a nival catchment. Thus, some sediment sources are connected late to the channel network.

During counter-clockwise looped events, sediment sources are widespread throughout the catchment and not exhausted rapidly. This is because the incorporation of sediment from areas that are not constantly connected to the channel network, like old debris-flow tails or unconsolidated deposition areas of older runoff events, trails, etc. These areas are only connected to the channel network when the runoff is generated all over the catchment. This is only possible under extremely high moisture conditions, so that saturation excess overland flow is generated independently of the topographical situation or by overflow of the widespread saturation areas that may function as storing tanks with only occasional connection to the channel network. This is the main difference between the first two flood types: the clockwise loop is generated under high but spatially limited moisture conditions (and limited contributing areas), whilst the counter-clockwise loop is brought about when there are soils near saturation all over the catchment and consequently the contributing areas are extended to the whole catchment.

The third group of floods, eight-shaped hysteresis, has only been described in a few publications (Arnborg et al., 1967; Williams, 1989). In the present case, the orientation of the loop is opposite: a counter-clockwise partial loop with low-flow followed by a clockwise loop with high discharge. In our case, the soil moisture of the catchment was far below saturation (around field capacity), where the hydraulic conductivity of the soil matrix is very low (Seeger, 2001). These circumstances, combined with high rainfall intensities, have lead to Hortonian overland flow, which can be considered the predominant process. Eight-shaped floods can be understood as a sequence of clockwise and counter-clockwise partial floods. At the first stage, flood generation and sediment production occurs near the channel, as observed and described by clockwise hysteresis loops. In these flat valley bottom areas, vertic and stagnic conditions of the soil are dominant, and low infiltration capacities were measured. These areas could be activated by saturation via the concentration of flow and interflow processes through the cracks of the clayey soils (Seeger, 2001), especially when macropore flow is understood as a kinematic wave (Germann, 1985; Germann and Beven, 1985). When the macropores of the shallow soils are saturated, in combination with high rainfall intensities, the total infiltration capacity of the soil is controlled by the transport capacity of the macropore-system and the infiltration capacity of the matrix. The latter is very low due to its low water content. So, the contributing areas are extended all over the catchment, showing a generalised Hortonian overland flow generation. At this stage of the flood, a counter-clockwise shaped partial hysteresis loop can be observed. In fact, during eight-shaped floods *SSC* is nearly as high as during counter-clockwise floods (Table 1). As the intensity of the rainfall decreases, the generation of Hortonian overland flow stops and the contributing areas are closer to the ravine where sediment sources are limited and rapidly exhausted during the event. As a consequence, sediment production decreases faster than runoff generation and the hysteresis loop runs clockwise again.

The DCA not only extracts the factors determining the shape of the hysteretic loop (the catchment soil water content, the total precipitation amount and the mid term antecedent rainfall), but it also makes clear

that the average soil moisture is the main factor steering the processes of runoff generation and sediment transport.

The ANOVA confirms the conclusions of the DCA, where the soil moisture is the only significant factor to differentiate all types of hysteretic loops, whereas the total rainfall amount of the event and the antecedent rainfall may contribute to change the normal situation with clockwise hysteretic loops of sediment transport to the other types.

The present study shows that clockwise hysteretic loops of the *Q-SSC* relationship are the common types of sediment transport in this catchment of the Mediterranean mountains. However, under certain conditions, counter-clockwise shaped hysteretic loops and even eight shaped may occur. The occurrence of the different types of loops is only dependent on three factors, the total precipitation of the event, the antecedent precipitation and the soil moisture. Here the soil moisture is the only significant differentiating factor, that explains nearly 80% of the variance of the three classes of flood types. So, eight-shaped hysteretic loops are generated under dry soil moisture conditions, whilst counter-clockwise shaped events are generated under extreme moist conditions of the catchment. It can be deduced from this that the hysteretic loops are expressions of different runoff generation processes and of changes in contributing areas.

Acknowledgements

References

Arnáez, J., Martí-Bono, C., Beguería, S., Lorente, A., Errea, M.P., García-Ruiz, J.M., 1999. Factores en la generación de crecidas en una cuenca de campos abandonados, Pirineo Central Español. Cuadernos de Investigación Geográfica 25, 7–24.

Arnborg, L., Walker, H.J., Peippo, J., 1967. Suspended load in the Colville River, Alaska, 1962. Geografiska Annaler 48A (2–4), 131–144.

Batalla, R.J., Sala, M., 1994. Temporal variability of suspended sediment transport in a Mediterranean sandy gravel-bed river. Variability in Stream Erosion and Sediment Transport. IAHS Publ. 244, IAHS, Canberra, 1994, pp. 299–305.

Bronstert, A., 1994. Modellierung der Abflussbildung und der Bodenwasserdynamik von Hängen. IHW, 46. Institut für Hydrologie und Wasserwirtschaft, Karlsruhe.

Bronstert, A., Glüsing, B., Plate, E., 1998. Physically-based hydrological modelling on the hillslope and micro-catchment scale: examples of capabilities and limitations. Hydrology, Water Resources and Ecology in Headwaters (HeadWater'98 Conference), 207–215.IAHS publ. IAHS, Meran/Merano.

Chikita, K.H., Kemnitz, R., Kumai, R., 2002. Characteristics of sediment discharge in the subarctic Yukon River, Alaska. Catena 48, 235–253.

DeBoer, D.H., Campbell, I.A., 1989. Spatial scale dependence of sediment dynamics in a semi-arid badland drainage basin. Catena 16, 277–290.

diCenzo, P.D., Luk, S.-h., 1997. Gully erosion and sediment transport in a small subtropical catchment. Catena 29, 161–176.

FAO, ISRIC and ISSS, 1998, World reference base of soil resources. World Soil Resources Reports, 84. Rome. 109 pp.

Gallart, F., Latron, J., Regüés, D., 1998. Hydrological and sediment processes in the research catchments of Vallcebre (Pyrenees). In: Boardman, J., Favis-Mortlock, D. (Eds.), Modelling Erosion by Water, NATO-ASI series 1-55, Springer, Berlin, pp. 503–511.

García-Ruiz, J.M., Martí-Bono, C., Arnáez-Vadillo, J., Beguería-Portugués, S., Lorente-Grima, A., Seeger, M., 2000. Las cuencas experimentales de Arnás y San Salvador en el Pirineo Central Español: escorrentía y transporte de sedimento. Cuadernos de Investigación Geográfica 26, 23–40.

Germann, P.F., 1985. Kinematic wave approach to infiltration and drainage into and from soil macropores. Transactions of the ASAE 28 (3), 745–749.

Germann, P.F., Beven, K.J., 1985. Kinematic wave approximation to infiltration into soils with sorbing macropores. Water Resources Research 21 (7), 990–996.

Hargreaves, G.H., Samani, Z.A., 1985. Reference crop evapotranspiration from temperature. Engineering Applied in Agriculture 1 (2), 96–99.

Havans, A.V., 1956. Using climatic data to estimate water in soil. New Jersey Agriculture 38, 6–10.

Hewlett, J.D., Hibbert, A.R., 1967. Factors affecting the response of small watersheds to precipitation in humid regions. In: Sopper, W.E., Lull, H.W. (Eds.), Forest Hydrology, Pergamon Press, Oxford, pp. 275–290.

Hodkins, R., 1999. Controls on suspended-sediment transfer at a high-arctic glacier, determined from statistical modelling. Earth Surface Processes and Landforms 24, 1–21.

Jansson, M.B., 2002. Determining sediment source areas in a tropical river basin, Costa Rica. Catena 47, 63–84.

Klein, M., 1984. Anti-clockwise hysteresis in suspended sediment concentration during individual storms. Catena 11, 251–257.

Kobayashi, D., Ishii, Y., Kodama, Y., 1999. Stream temperature, specific conductance and runoff process in mountain watersheds. Hydrological Processes 13, 865–876.

Lanfer, N., 1995. Wasserbilanz und Bestandsklima als Grundlage einer agrarklimatischen Differenzierung in der COSTA Ecuadors. Göttinger Beiträge zur Land-und Forstwirtschaft in den Tropen und Subtropen, 104, Göttingen, 204 pp.

Lenzi, M., Marchi, L., 2000. Suspended sediment load during floods in a small stream of the Dolomites (northeastern Italy). Catena 39, 267–282.

Llorens, P., Queralt, L., Plana, F., Gallart, F., 1997. Studying solute and particulate sediment transfer in a small mediterranean mountainous catchment subject to land abandonment. Earth Surface Processes and Landforms 22, 1027–1035.

Lorente, A., Martí-Bono, C., Beguería, S., Arnáez, J., García-Ruiz, J.M., 2000. La exportación de sedimento en suspensión en una cuenca de campos abandonados. Pirineo Central Español. Cuaternario y Geomorfología 14 (1–2), 21–34.

Pfau, R., 1966. Ein Beitrag zur Frage des Wasserhaushaltes und der Beregnungsbedürftigkeit landwirtschaftlich genutzter Böden im Raume der Europäischen Wirtschaftsgemeinschaft. Meteorologische Rundschau 19, 33–46.

Regüés, D., Balasch, J.C., Castelltort, X., Soler, M., Gallart, F., 2000. Relación entre las tendencias temporales de producción y transporte de sedimentos y las condiciones climáticas en una pequeña cuenca de montaña mediterránea (Vallcebre Pirineos Orientales). Cuadernos de Investigación Geográfica 26, 41–65.

Ries, J.B., Marzolff, I., Seeger, M., 2000. Der Einfluss von Beweidung auf die Vegetationsbedeckung und Bodenerosion in der Flyschzone der spanischen Pyrenäen. In: Zollinger, G., (Ed.), Aktuelle Beiträge zur angewandten physische Geographie der Tropen, Subtropen und der Regio Trirhena, Freiburger Geographische Hefte. Institut für Physische Geographie, Albert-Ludwigs-Universität Freiburg i. Br., Freiburg i. Br, pp. 167–194.

Sauer, T., Ries, J.B., 2002. The water balance of different soils on abandoned fields along a transect from the High Pyrenees to the Central Ebro Basin. In: García-Ruiz, J.M., Jones, J.A.A., Arnáez, J. (Eds.), Environmental change and water sustainability, Instituto Pirenaico de Ecología, CSIC, Zaragoza, pp. 99–109.

Seeger, M., 2001. Boden und Bodenwasserhaushalt als Indikatoren der Landdegradierung auf extensivierten Nutzflächen in Aragón/Spanien. Freiburger Geographische Hefte, 63. Institut für Physische Geographie, Albert-Ludwigs-Universität Freiburg i. Br., Freiburg i. Br., 184 + 30 pp.

Thornthwaite, C.W., Mather, J.R., 1957. Instructions and tables for computing potential evapotranspiration and water balance. Publications in Climatology 10, 243–311.

Threlfall, J., 1986. The relationship between discharge and susended sediment in a small nival subarctic catchment. In: Gardiner, V., (Ed.), International Geomorphology, Wiley, New York, pp. 823–841.

Williams, G.P., 1989. Sediment concentration versus water discharge during single hydrologic events in rivers. Journal of Hydrology 111, 89–106.